ISSN (Print) 1226-1750
ISSN (Online) 2233-6656
Journal of Magnetics 24(2), 217-222 (2019) https://doi.org/10.4283/JMAG.2019.24.2.217

Analysis of Magnetic Resonance Signals from Diffusion Weighted Imaging using Compressed Sensitivity Encoding Technique

Ji-Sung Jang[1,2], Yong-Soo Han[3,4], and Mi-Ae Jeong[5]*

[1]*Department of Radiology, Asan Medical Center, Seoul 05505, Korea*
[2]*Department of Biomedical Science, Korea University, Sejong 30019, Korea*
[3]*Department of Radiological Science, Hallym Polytechnic University, Chuncheon 24210, Korea*
[4]*Department of Medical Device Industry Dongguk-University, Seoul 04620, Korea*
[5]*Department of Dental Hygiene, Kangwon National University, Samcheok 25913, Korea*

(Received 13 February 2019, Received in final form 11 April 2019, Accepted 11 April 2019)

The purpose of this study was to compare image quality between compressed sensitivity encoding (CS) and sensitivity encoding (SENSE) in single-shot turbo spin echo diffusion-weighted imaging (TSE-DWI). Signal-to-noise ratios (SNR), apparent diffusion coefficient (ADC) values, and geometric accuracies were measured with an American College of Radiology head phantom. CS showed a high mean SNR, less variation in ADC values, and reduced imaging acquisition time (21.7 %-39.3 %) compared with SENSE. In addition, there was no significant difference in geometric accuracy between SENSE and CS. In conclusion, in comparison with SENSE TSE-DWI, CS TSE-DWI resulted in a reduced imaging acquisition time and improved SNR, while maintaining image quality.

Keywords : magnetic resonance imaging, magnetic resonance signal to noise ratio, sensitivity encoding, geometric accuracy

1. Introduction

Diffusion-weighted imaging (DWI) using single-shot echo-planar imaging (EPI) is the magnetic resonance (MR) imaging method most commonly used to diagnose early brain infarction and acute brain stroke. Not only is it fast and relatively insensitive to patient motion, it also has high sensitivity to acute ischemia and provides useful quantitative information on Brownian motion of water molecules in relation to normal or abnormal tissue [1, 2]. The apparent diffusion coefficient (ADC) obtained with DWI is also highly effective for differentiating tumor grades [3]. However, some studies have shown that EPI-DWI based on a spin echo sequence is subject to a low signal-to-noise ratio (SNR), low spatial resolution, and distortions (such as blurring and susceptibility artifact) due to eddy currents, the long echo planar imaging read out, and static magnetic field inhomogeneity [4-6]. In EPI-DWI, the above-mentioned artifacts can cause inaccurate ADC values and degrade image quality [7, 8]. To address this issue, other MRI sequences have been utilized for DWI, including single-shot turbo spin echo (TSE-DWI). TSE-DWI demonstrated reduced image distortion and chemical shift artifacts in comparison with EPI-DWI [9], although it is subject to a low SNR and severe image blurring in the phase-encoding direction [10].

A study by Yoshida *et al.* evaluated the relationship between the image quality of TSE-DWI and various sensitivity encoding (SENSE) acceleration factors (AFs) [11], and recent advances in combining compressed sensing and SENSE-based parallel imaging (PI) techniques, so called compressed SENSE (CS), can reduce scan times further than conventional PI techniques, while maintaining image quality [12, 13]. However, there is currently no report directly comparing CS and conventional SENSE TSE-DWI sequences. We hypothesized that TSE-DWI using CS can reduce scan time without sacrificing image quality compared to the TSE-DWI using SENSE. Therefore, the purpose of this study was to compare image quality between CS and SENSE in TSE-DWI.

*Corresponding author: Tel: +82-33-540-3391
Fax: +82-33-540-3399, e-mail: teeth2080@kangwon.ac.kr

2. Background

Magnetic resonance imaging (MRI) is a widely used and essential modality for anatomical and functional diagnosis. Although MRI has a high resolution in all areas of the body, the primary disadvantage of MRI is that it requires a relatively long scan time compared with other medical imaging modalities such as computed tomography or ultrasound. To reduce the acquisition time for conventional MRI, PI techniques were developed to reduce the phase-encoding steps required and enable faster MR data acquisitions. One of the most commonly used conventional PI techniques is SENSE, which unfolds superimposed pixels in the image domain. The SENSE technique is based on the fact that the receiver sensitivity generally has an encoding effect of its own due to the simultaneous acquisition of data from multiple receiver arrays with spatially varying sensitivities. The acceleration factor (AF) is the ratio between the number of k-space lines of fully acquired image and an image acquired with PI technique such as SENSE. Thus, SENSE reduces the number of Fourier-encoding steps required and allows collection of more data without additional scan time [14]. The SENSE equation is shown in Eq. (1).

$$p = \min_{p}\left(\sum_{i=1}^{\#coils} \left\| m_{d,i} - ES_{d,iP} \right\|_2^2 \right) + \lambda_1 \left\| R^{-1/2} P \right\|_2^2 \qquad (1)$$

where p is the reconstructed image, $m_{d,i}$ is the measured data for a given coil element after noise decorrelation, E is the under-sampled Fourier operator as defined by the sampling pattern, $S_{d,i}$ is the coil sensitivity for a given coil element after the noise decorrelation obtained from the SENSE reference scan, λ_1 is a regulation factor allowing a balance between data consistency and prior knowledge of the image content, and R is a coarse resolution image from the integrated body coil that is obtained with the SENSE reference scan.

The CS acquisition involves a combination of compressed sensing and SENSE to obtain a balanced incoherent under-sampled acquisition of variable density, and then iterative reconstruction to remove the aliasing artifact, thereby resulting in a clean image without artifact [12, 13, 15]. The main difference between SENSE and CS is that the CS image is transformed into the wavelet domain, where information in the image is represented at different spatial scales and can be relatively sparse. This means that the image information is acquired more efficiently, and the scan time can be reduced. The formula for CS is given in Eq. (2) [13].

$$p = \min_{p}\left(\sum_{i=1}^{\#coils} \left\| m_{d,i} - ES_{d,iP} \right\|_2^2 \right) + \lambda_1 \left\| R^{-1/2} P \right\|_2^2 + \lambda_2 \left\| \Psi P \right\|_1 , \qquad (2)$$

where λ_2 is a regulation factor to balance the sparsity constraining and data consistency in the iterative solution, and Ψ is the sparsity transform into the wavelet domain.

The simple diagram indicating principle of the SENSE and CS technique are shown in Fig. 1.

3. Materials and Methods

3.1. Phantom study

An MR phantom accredited by the American College of Radiology (ACR; JM, Specialty Parts, San Diego, CA, USA) was used for the phantom measurements performed in this study. The internal measurements of the ACR phantom were 148 mm in length and 190 mm in diameter. The phantom was filled with a solution of nickel chloride

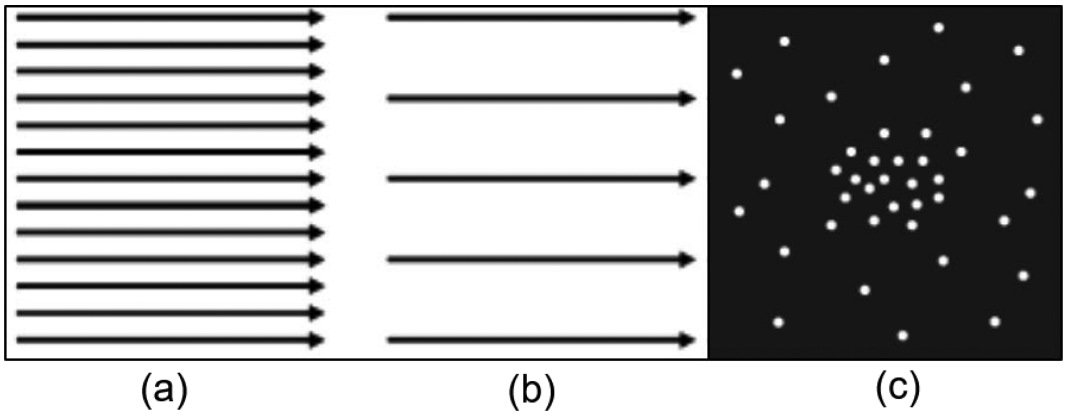

Fig. 1. A simple diagram indicating the principles of filling k-space in the SENSE and CS technique. (a) Uniformly sampled k-space without SENSE (b) Uniformly under-sampled k-space using SENSE (acceleration factor-3) (c) Incoherently under-sampled k-space with variable density in CS technique.

Table 1. Summary of the single-shot turbo spin echo diffusion-weighted imaging parameters.

	SENSE				Compressed SENSE			
AF	2.0	3.0	4.0	5.0	4.0	5.0	6.0	7.0
TR (ms)	4828	3542	2868	2501	2933	2554	2238	2048
TE (ms)	63	63	63	63	63	63	63	63
Shot duration (ms)	362	245	184	150	189	155	126	109
Time (s)	193	142	115	100	117	102	90	82

AF, acceleration factor; TR, repetition time; TE, echo time.

and sodium chloride (10 mM $NiCl_2$ and 75 mM NaCl [16]), and was carefully aligned and positioned in the center of each head coil in a spatial orientation defined according to its nose and chin marks. The scanning was performed at room temperature (21.0 °C) to avoid any problems with temperature dependence of the quantitative measurements. Given that this was a phantom study, written informed consent was not applicable.

3.2. MR protocol

All scans were performed on a clinical 3-Tesla MR scanner (Ingenia, Philips Healthcare, The Netherlands) using 32-channel head coils (Philips Healthcare). No image signal intensity corrections were applied when the TSE-DWI sequences were used. TSE-DWI acquisitions with two b-values (0 and 1000 s/mm^2) were acquired in the axial plane. The TSE-DWI scanning parameters included field of view: 230 × 230 mm; voxel size: 1.8 × 1.8 mm; acquisition matrix: 128 × 128; reconstruction matrix: 256 × 256; flip angle: 90°; time of repetition (TR): shortest; time of echo (TE): shortest; slice thickness: 5 mm; slice gap: 5 mm; number of slices: 11; SENSE AFs: 2, 3, 4, and 5; CS AFs: 4, 5, 6, and 7; number of acquisitions (NSA): 4. The phase-encoding direction was left to right. A detailed summary of the TSE-DWI parameters is presented in Table 1. The slice thickness and slice gap were set according to the ACR phantom test guidelines [16].

3.3. Image analysis

The MR imaging data for each b-value were transferred from the picture archiving and communication system to a personal computer. The SNR analysis was performed on slice 7 of the ACR phantom, where the image contrast was uniform. The SNR values were calculated from each b = 1000 s/mm^2 TSE-DWI acquisition using the National Electrical Manufacturers' Association subtraction method 1 [17], according to the following equation:

$$SNR = \frac{S}{\sigma/\sqrt{2}}, \quad (3)$$

where S is the mean signal value of two images and σ is the standard deviation of the subtracted images. S and σ were derived from corresponding regions of interest (ROI) on the two images and the subtracted image. The $\sqrt{2}$ factor arises because noise with a propagation of error is derived from the difference image [17, 18]. Image analysis was performed using ImageJ (ImageJ v. 1.45; National Institutes of Health, Bethesda, MD, USA).

ADC values obtained from TSE-DWI with different SENSE and CS AFs were calculated according to the following equation:

$$ADC = \frac{1}{(b_2 - b_1)} \log_e\left[\frac{S_1}{S_2}\right], \quad (4)$$

where S_1 and S_2 are signal intensities acquired at the low b-value b_1 and the high b-value b_2, respectively. To assess geometric accuracy, the diameter of the phantom image on slice 5 was measured in four directions: top-to-bottom, left-to-right, and along both diagonals.

3.4. Statistical analysis

The SNR values obtained from the TSE-DWI using SENSE and CS were compared using a paired Student's *t*-test. Statistical analyses were performed using IBM SPSS Statistics for Windows/Macintosh Version 21.0 (IBM Corp., Armonk, NY, USA). For all statistical analyses, a two-sided probability level of $p < 0.05$ was considered statistically significant. The coefficient of variance (CV) was used to evaluate the precision of repeated measures of geometric accuracy and ADC values obtained from the SENSE and CS imaging. The CV of five repeated measurements was calculated by dividing the standard deviation by the mean length values.

4. Results

The SNR values showing the relationship between SNR and AF in the TSE-DWI using SENSE and CS are presented in Fig. 2. In general, in TSE-DWI using either SENSE or CS, the SNR values tended to decrease as the AF increased. The highest SNR from the TSE-DWI using

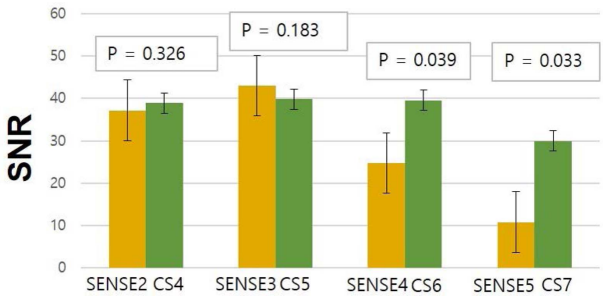

Fig. 2. (Color online) Signal-to-noise ratio (SNR) measurements on TSE-DWI as a function of CS and SENSE.

SENSE was measured at a SENSE AF of 3, while a CS AF of 5 showed the highest SNR. In TSE-DWI using SENSE, the mean SNR values at SENSE AFs of 4 and 5 were reduced by 33.4 % and 71.1 %, respectively, compared with a SENSE AF of 2. With the TSE-DWI using CS, the mean SNR reductions were 0.6 % and 24.8 % at CS AFs of 6 and 7, respectively, compared with a CS AF of 4. Comparison of SENSE with CS showed no statistically significant differences between a SENSE AF of 2 and a CS AF of 4, and a SENSE AF of 3 and a CS AF of 5 ($p > 0.05$). However, there were statistically significant differences between a SENSE AF of ≥ 4 and a CS AF of ≥ 6 ($p < 0.05$; Fig. 2).

Fig. 3 shows ADC maps calculated from the TSE-DWI using SENSE and CS. Increasing image noise was observed as AF increased, especially at AFs of 4 and 5 in the TSE-DWI using SENSE. However, reduced image noise was observed at CS AFs of 6 and 7 in comparison with SENSE AFs of 4 and 5. Table 2 shows the mean ADC values and CVs obtained from the TSE-DWI using SENSE and CS. Contrary to the findings with CS, the mean ADC values obtained from the TSE-DWI using SENSE tended to decrease as AF increased. In addition, SENSE showed a greater variation than CS in the mean ADC values. However, the repeatability of ADC values was good in TSE-DWI using either SENSE or CS, with all CVs being within 1.06 %.

Fig. 4 demonstrates the geometric accuracy of slice 5 images obtained from the TSE-DWI using SENSE and CS. All measured lengths in the TSE-DWI using SENSE and CS were within ± 2 mm of their true diameters, and all their CV values were within 0.21 %. However, image blurring in the phase-encoding direction was reduced as the AF increased in both SENSE and CS imaging, despite image noise increasing as the AF increased.

Table 2. The apparent diffusion coefficient (ADC) values and coefficients of variation (CV) of the ADCs obtained with single-shot turbo spin echo diffusion-weighted imaging (TSE-DWI) using SENSE and compressed SENSE.

Acquisition techniques	ADC (10^{-3} mm^2s^{-1})	CV (%)
SENSE 2	2.155 ± 0.021	0.98
SENSE 3	2.153 ± 0.021	0.97
SENSE 4	2.141 ± 0.022	1.06
SENSE 5	2.076 ± 0.011	0.55
CS 4	2.142 ± 0.029	0.38
CS 5	2.156 ± 0.022	1.06
CS 6	2.152 ± 0.019	0.89
CS 7	2.164 ± 0.021	0.93

SENSE, sensitivity encoding; CS, compressed SENSE; ADC, apparent diffusion coefficient; CV, coefficient of variation.
ADC values are expressed as mean ± standard deviation.

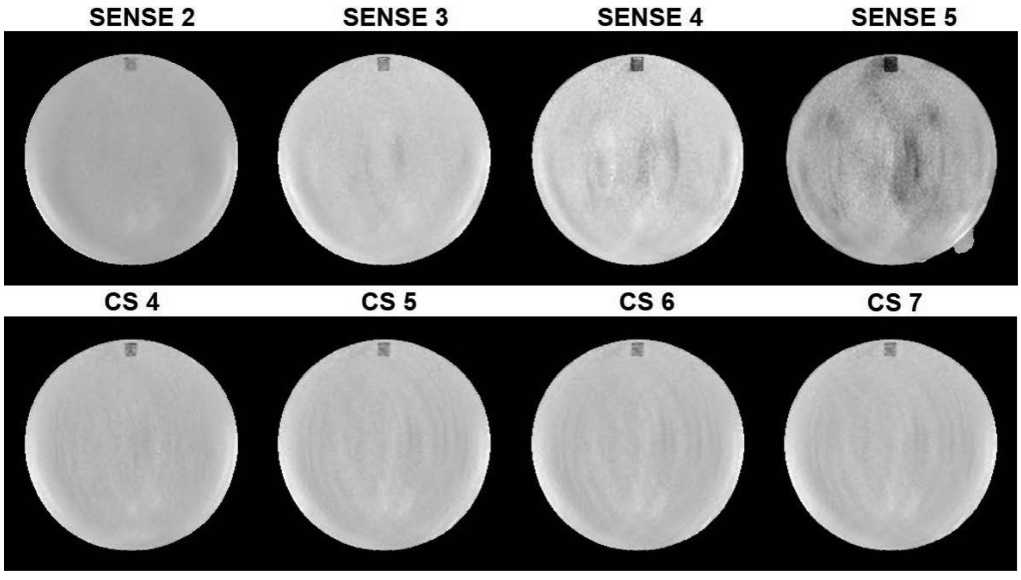

Fig. 3. Apparent diffusion coefficient (ADC) maps obtained from TSE-DWI using CS and SENSE.

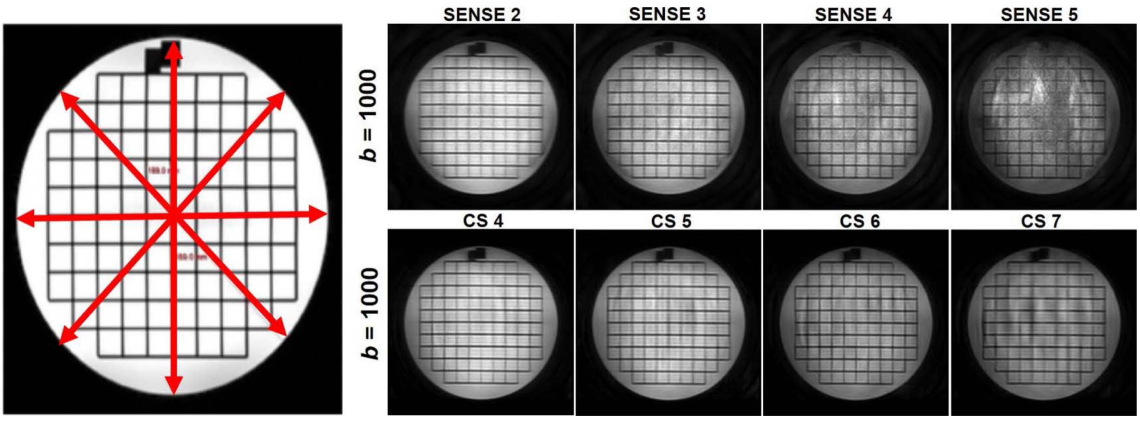

Fig. 4. (Color online) Phantom images used for evaluating geometric accuracy on slice 5 as a function of CS and SENSE.

Table 3. The coefficients of variation (CV) and quantitative results of measurements of geometric accuracy on slice 5.

		SENSE				Compressed SENSE			
	AF	2.0	3.0	4.0	5.0	4.0	5.0	6.0	7.0
TB	Length (mm)	189.27 ± 0.18	189.41 ± 0.16	189.21 ± 0.16	189.07 ± 0.09	189.21 ± 0.16	189.13 ± 0.09	189.13 ± 0.09	189.53 ± 0.24
	CV (%)	0.09	0.08	0.08	0.04	0.08	0.04	0.04	0.13
LR	Length (mm)	189.61 ± 0.16	189.21 ± 0.09	189.11 ± 0.04	188.39 ± 0.24	189.33 ± 0.09	189.36 ± 0.12	189.26 ± 0.09	189.53 ± 0.24
	CV (%)	0.08	0.04	0.02	0.13	0.04	0.06	0.04	0.13
UR to LL	Length (mm)	189.26 ± 0.41	189.61 ± 0.35	188.29 ± 0.32	188.06 ± 0.24	188.23 ± 0.18	188.43 ± 0.21	188.46 ± 0.22	188.53 ± 0.21
	CV (%)	0.21	0.18	0.16	0.12	0.09	0.11	0.11	0.11
UL to LR	Length (mm)	189.11 ± 0.14	189.13 ± 0.04	188.53 ± 0.24	188.73 ± 0.16	189.43 ± 0.21	189.21 ± 0.28	188.86 ± 0.04	189.23 ± 0.23
	CV (%)	0.07	0.02	0.13	0.08	0.11	0.14	0.02	0.12

TB, top to bottom; LR, left to right; UR, upper right; UL, upper left; LL, lower left; LR, lower right.
Length values are expressed as mean ± standard deviation.

5. Discussion

In this study, we analyzed the SNR and ADC values obtained from TSE-DWI using CS and SENSE. In addition, we measured geometric accuracy to evaluate image distortion on TSE-DWI using CS and SENSE. In comparison with TSE using SENSE, CS significantly reduced the TSE scan time while maintaining or improving image quality. In particular, a CS AF of 4 demonstrated similar SNRs to a SENSE AF of 2, with a reduction in scan time of 40 %. Previous reports showed that higher AFs not only increased noise amplification or the average g factor, but also had a considerable negative influence on the SNR [14, 19]. These previous results were similar to our findings showing that the SNR decreased as the AF increased, with either CS or SENSE. However, the overall SNR of the TSE-DWI using CS was higher than that using SENSE. This may be supported by the iterative reconstruction from variable-density random under-sampling of k-space data, which may contribute to improvements in the SNR [12].

Increasing the NSA is one way to improve the SNR in TSE-DWI. However, this requires a long scan time, which can result in patient motion. To address this weakness, increased NSA with CS should be considered in comparison with increased NSA with SENSE. A prolonged scan time caused by an increase in NSA can be reduced by the use of CS, which can compensate for the relatively low SNR of TSE-DWI; our results demonstrated that CS can reduce scan time while maintaining image quality in comparison with SENSE. Thus, it is important to use an appropriate AF and understand the relationship between SENSE or CS and the image quality of TSE-DWI.

Our study also demonstrated the variability of ADC values and geometric accuracy measurements obtained from TSE-DWI using SENSE and CS. The reproducibility of the ADC values obtained with TSE-DWI was similar to that reported in a recent study, regardless of whether SENSE or CS were used [11]. In addition, the CV values of geometric accuracy measurements were good with both CS and SENSE. All measured lengths on CS and SENSE images were within ± 2 mm of their true

values, with there being no significant differences in geometric accuracy between CS and SENSE. Furthermore, reduced image blurring in the phase-encoding direction was observed as AF increased in both CS and SENSE, although the increase in AF led to an increase in image noise. This is consistent with the results of a recent study [11] and could be explained by the fact that the higher AF reduces the shot duration, which causes image blurring owing to T_2 decay in the phase-encoding direction. Considering the above-mentioned findings, TSE-DWI using CS maintains geometric accuracy, provides less variation in ADC values, and reduces scanning time in comparison with TSE-DWI using SENSE.

There were some limitations to our study. First, it was based on the ACR phantom, which is mainly used for quality assurance and does not simulate lesions with low ADC values such as acute stroke and glioma. Second, our experiment was conducted using only one type of MR scanner at a single center. Previous studies have reported that different equipment and field strengths have different effects on the SNR and ADC values of DWI [7, 8]. Therefore, further studies should be performed to evaluate the effects of different MR scanner types and field strengths. Lastly, although the shortest TR values were used in both SENSE and CS techniques, there were differences in TR between SENSE and CS, due to mechanical constraints of acquisition techniques. Nevertheless, this is the first study comparing the image quality of TSE-DWI using SENSE and CS. In addition, this study provides baseline information related to the use of CS in MRI, which could be of use in a diverse array of medical MRI fields.

6. Conclusion

In conclusion, TSE-DWI using CS enabled a reduction in the imaging acquisition time while maintaining image quality and improving SNR in comparison with TSE-DWI using SENSE. However, CS AFs of 6 and 7 were subject to substantial image noise, despite having a higher SNR than SENSE with AFs of 4 and 5. Optimizing the use of CS in TSE-DWI can provide a similar image quality to that of TSE-DWI using SENSE, with a comparative reduction in scan time.

References

[1] D. Saur, T. Kucinski, U. Grzyska, B. Eckert, C. Eggers, *et al*., AJNR Am. J. Neuroradiol. **24**, 878 (2003).
[2] Q. Cheng, X. Xu, Q. Zu, S. Lu, J. Yu, *et al*., Exp. Ther. Med. **12**, 951 (2016).
[3] S. J. Ahn, S. H. Choi, Y. J. Kim, K. G. Kim, C. H. Sohn, *et al.*, Acad. Radiol. **19**, 1233 (2012).
[4] P. Jezzard and S. Clare, Hum. Brain. Mapp. **8**, 80 (1999).
[5] P. Jezzard and R. S. Balaban, Magn. Reson. Med. **34**, 65 (1995).
[6] J. N. Morelli, M. R. Saettele, R. A. Rangaswamy, L. Vu, C. M. Gerdes, *et al.*, J. Clin. Imaging. Sci. **2**, 31 (2012).
[7] A. S. Kivrak, Y. Paksoy, C. Erol, M. Koplay, S. Özbek, and F. Kara, Diagn. Interv. Radiol. **19**, 433 (2013).
[8] I. Lavdas, M. E. Miquel, D. W. McRobbie, and E. O. Aboagye, J. Magn. Reson. Imaging. **40**, 682 (2014).
[9] D. C. Alsop, Magn Reson Med. **38**, 527 (1997).
[10] J. Sakamoto, M. Otonari-Yamamoto, and K. Nishikawa, T. Sano. Oral Radiol. **28**, 87 (2012).
[11] T. Yoshida, A. Urikura, K. Shirata, Y. Nakaya, S. Terashima, and Y. Hosokawa. Br J. Radiol. **89**, 1065 (2016).
[12] J. E Vranic, N. M. Cross, Y. Wang, D. S. Hippe, E. de Weerdt, and M. Mossa-Basha. AJNR Am. J. Neuroradiol. **40**, 92 (2019).
[13] L. Geerts-Ossevoort, d.W.E., A. Duijndam, G. Van Ijperen, H. Peeters, M. Doneva, M. Nijenhuis, A. Huang. [cited 2018 16 May]; Available from: https://philipsproductcontent.blob.core.windows.net/assets/20180109/619119731f2a42c4acd4a863008a46c7.pdf.
[14] K. P. Pruessmann, M. Weiger, M. B. Scheidegger, and P. Boesiger, Magn. Reson. Med. **42,** 952 (1999).
[15] I. Y. Chun, B. Adcock, and T. M. Talavage, IEEE Trans. Med. Imaging **35**, 354 (2016).
[16] Z. J. Wang, Y. Seo, J. M. Chia, and N. K. Rollins, Med. Phys. **38**, 4415 (2011).
[17] F. L. Goerner and G. D. Clarke, Med. Phys. **38**, 5049 (2011).
[18] M. J. Firbank, A. Coulthard, R. M. Harrison, and E. D. Williams, Phys. Med. Biol. **44**, 261 (1999).
[19] T. Yoshida, K. Shirata, A. Urikura, M. Ito, and Y. Nakaya, Radiol. Phys. Technol. **8**, 305 (2015).